Applied Acoustics 136 (2018) 86–93

Contents lists available at ScienceDirect

Applied Acoustics

journal homepage: www.elsevier.com/locate/apacoust

A microstructure material design for low frequency sound absorption

Thomas Dupont[a,*], Philippe Leclaire[a], Raymond Panneton[b], Olga Umnova[c]

[a] DRIVE EA1859, Univ. Bourgogne Franche Comté, ISAT, BP 31 - 49 rue Mlle Bourgeois, 58027 Nevers, France
[b] GAUS, Département de Génie Mécanique, Université de Sherbrooke, Sherbrooke J1K 2R1, Canada
[c] Acoustics Research Centre, University of Salford, Salford M5 4WT, United Kingdom

ARTICLE INFO

Keywords:
Low-frequency
Sound-absorber
Dead-end pore
Periodic array of resonators
Microstructure design
Bandgap effect

ABSTRACT

The acoustic properties of an air-saturated porous material depend on its microstructure and the thickness of the sample. Thick samples of conventional acoustic materials are required to achieve good absorption at low frequencies. This study suggests a new micro-structure for the design of low-frequency resonant acoustic absorbers. A perforated material is studied, in which the main perforations are connected to a collection of periodically spaced very thin annular dead-end pores with respect to the lateral size, these absorbers are called multi-pancake materials. It is shown, that at low frequencies, the periodic array of annular dead-end pores increases the effective compressibility without modifying the effective dynamic density. Due to this effect, the first sound absorption peak appears at much lower frequency, compared to that of the structure without dead-end pores. A transfer matrix approach is proposed to model and optimize the absorber. Prototypes have been 3D printed and tested for sound absorption and transmission loss. This design allowed to design materials capable of producing absorption peaks at a few hundred Hz and constituted of a stacking of 10–20 annular dead-end pores, each dead-end having a thickness of the order of 1 mm or less so that the overall material thickness was of a few cm. A good agreement between the data and the model predictions is demonstrated.

1. Introduction

The acoustic properties of an air-saturated porous material depend on its microstructure and on the thickness of the sample [1]. Conventional acoustic treatments (such as foams or fibrous materials) of large thickness are required to achieve good sound absorption at low frequencies, which leads to a reduction of the air space volume and a significant increase of the material price. The purely reactive treatments (such as quarter wavelength resonator or Helmholtz Resonator [2]) or the reactive and resistive materials (such as a microperforated plate (MPP) [3] or a resistive film coupled with a macro-perforated plate [4]) backed by an air cavity can be used to improve the absorption at medium frequencies. However, a large depth cavity is still required to achieve low frequency absorption. Hence, the development of thin acoustic materials for low frequency absorption is an important challenge for the industry and is required in many applications, e.g. the acoustic liners for turbo fan engine [5], the passenger compartments, or the acoustic treatments of buildings.

To improve the absorption at low frequencies, Li et al. [6] proposed to add some extended tubes to MPP. Lagarrigue et al. [7] proposed to insert periodic lattice of resonators in rigid porous material. Boutin [8] proposed to use the homogenization method to model the acoustic of porous media with inner resonators. Based on Bradley's works [9], Leclaire et al. [10] have studied a structured perforated material containing periodically spaced dead-end (DE) pores (such as quarter wavelength or Helmholtz resonators). It has been observed that the presence of a periodic lattice of dead-end pores leads to the appearance of absorption peaks at low frequencies and at high frequencies (bandgap or stop bands for the sound transmission). Similar observations on other sound absorbing systems were reported by Groby et al. [11].

In Ref. [10], it has been proposed to model the resonant material with periodically spaced dead-end cavities by a transfer matrix approach or using low frequency asymptotic expansions. The presence of the network of DE pores has the effect, at low frequencies, of increasing the effective compressibility of the material without changing its effective dynamic density. This induces a decrease of the effective celerity of the material (Groby et al. [11] suggest calling this kind of material "slow sound material"). Due to this effect, the presence of a periodic network of pores significantly reduces the resonance frequencies of the material. This leads to the appearance of the absorption peaks at much lower frequencies without increasing the thickness of the resonant material. The model has been validated by numerical simulation and by comparing its predictions with measurements on prototype samples.

Based on this work, we propose a new type of microstructure design

* Corresponding author.
E-mail address: thomas.dupont@u-bourgogne.fr (T. Dupont).

https://doi.org/10.1016/j.apacoust.2018.02.016
Received 19 October 2017; Received in revised form 9 February 2018; Accepted 14 February 2018

for low frequency resonant materials. In order to enhance the thermal effects at low frequencies and thus to decrease the first resonance frequency, the proposed microstructure is directly inspired by the design of heat exchangers. A perforated material with a periodic lattice of "pancake" cavities is designed and modeled. Here, "pancake cavities" is the name for very thin annular cavities (or ring cavities) with respect to the lateral sizes of the annuli, so that the ratio between annulus radius and thickness can be high (for example 40 or more). Another advantage of the ring cavities is that their volume can be significantly larger than that of the previously considered DE pores of Ref. [10], which is an advantage to reduce the frequencies of the absorption peaks. In the first part of the paper, the expressions of the low frequency approximation of effective parameters of this kind of material are presented and the design of the microstructure is proposed. Several prototypes are presented and the fabrication process is discussed. A model based on the transfer matrix formulation is described in the second part. The determination of the pancake cavity impedance is inspired by the work of Dickey and Selamet [12] on the acoustic behavior of a Helmholtz resonator with a "pancake" shape. Then, in the third part, numerical and experimental validations of the model are presented. A patent application has been filed on the thin multi-pancake resonant materials [13].

2. Material and methods

2.1. Proposed design for the microstructure of a resonant material

2.1.1. Low frequency approximation and effective parameters

An example of material with periodically distributed DE pores, proposed in Ref. [10], is presented in Fig. 1. When the distance between neighboring dead-end pores is small compared to the wavelength of sound in the main pore, the expressions for the effective density and compressibility of the material have been derived. A simple self-consistent model similar to a coherent potential approximation [14] has been used. For the design shown in Fig. 1, the low frequency expression of effective dynamic density ρ_e and effective compressibility C_e are given by the following equations [10]:

$$\rho_e = \rho_{mp}, \tag{1}$$

$$C_e = C_{mp} + C_{de}\frac{NA_{de}}{A_{mp}}\frac{d}{h}\left(\frac{\tan(k_{de}d)}{k_{de}d}\right), \tag{2}$$

where ρ_{mp} and C_{mp} are the effective density and effective compressibility of air in the main pore and ρ_{de} and C_{de} are the effective density and effective compressibility of air in DE pores, $k_{de} = \omega\sqrt{\rho_{de}C_{de}}$ is the wavenumber in DE pores, and ω is the angular frequency. These effective parameters can be expressed using an equivalent fluid model (for example JCA approach [1]). The geometrical parameters of the pores are: A_{mp} the cross-sectional area of the mean pore, h the periodicity, i.e. centre-to-centre distance between two neighboring DE pores, A_{de} and d are the cross-sectional area and the length of the DE pores. N is number of DE pores per period h.

Moreover, if Re $(k_{de}d) \ll 1$ (very low frequency and/or short DE pores), the expression for the compressibility can be reduced to:

$$C_e = C_{mp} + C_{de}\frac{NA_{de}}{A_{mp}}\frac{d}{h} = C_{mp} + C_{de}\frac{V_{de}}{V_{mp}}, \tag{3}$$

with V_{mp} and V_{de} the total volumes of the main and of the DE pores per period h.

According to Eqs. (1)–(3), a periodic array of DE pores at low frequencies does not modify the effective density of air in the main pore, but it increases significantly its effective compressibility. That means that the periodic array of DE pores has a significant influence on thermal effects in the thermal boundary layers near the DE pore walls as the effective compressibility ($C_e = 1/K_e$ with K_e the effective Bulk modulus) is generally associated to them [15].

Moreover, the low frequency approximation of the effective sound speed is given by:

$$c_e = \frac{1}{\mathrm{Re}\left(\sqrt{\rho_e C_e}\right)} \xrightarrow[\mathrm{Re}(k_{de}d)\ll 1]{} \frac{1}{\mathrm{Re}\left(\sqrt{\rho_e\left(C_{mp} + C_{de}\frac{V_{de}}{V_{mp}}\right)}\right)}, \tag{4}$$

It is clear from this equation, that periodic array of DE pores decreases sound speed in the material.

If we consider a quarter-wavelength thickness L material with straight main pores only, the first resonance frequency is given by:

$$f_{res1} = \frac{c_{mp}}{4L}, \tag{5}$$

where c_{mp} *is* the effective sound speed in the main pore. If a periodic array of lateral DE pores is added, the effective sound speed c_e is given by Eq. (4), and the first resonance frequency is modified as follows:

$$f^*_{res1} = \frac{1}{4L}\frac{1}{\mathrm{Re}\left(\sqrt{\rho_e\left(C_{mp} + C_{de}\frac{V_{de}}{V_{mp}}\right)}\right)}, \tag{6}$$

Thus periodic array of DE pores reduces the first resonance frequency in a significant way.

2.1.2. Proposed design

Based on the low frequency model presented in the previous section (Eqs. (3) and (6)), it is proposed here to optimize the microstructure of the DE pores in order to achieve the first resonant frequency (of perforated material) as low as possible without changing the main pore geometry and the sample thickness. It follows from (Eq. (6)), that in

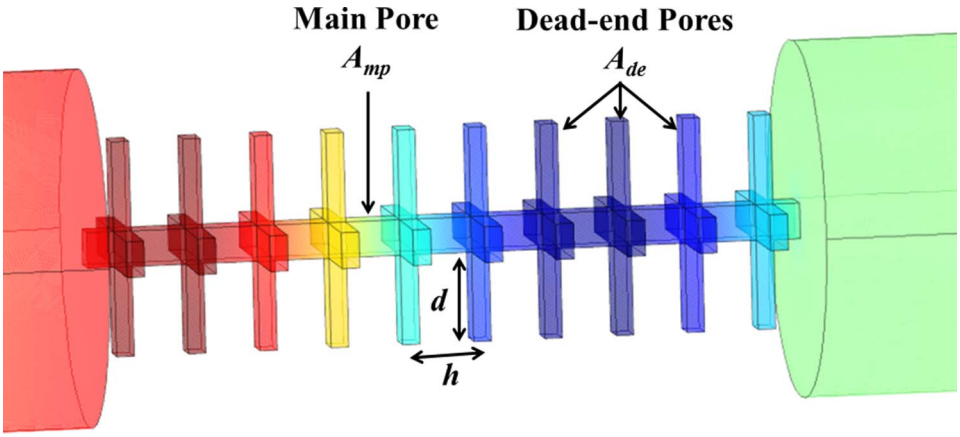

Fig. 1. Main pore (with a cross-sectional area A_{mp}) with periodically arranged dead-end pores, $N = 4$ identical dead-end pores with cross-section area A_{de} and length d per period h. The dead-end pores are located at "nodes".

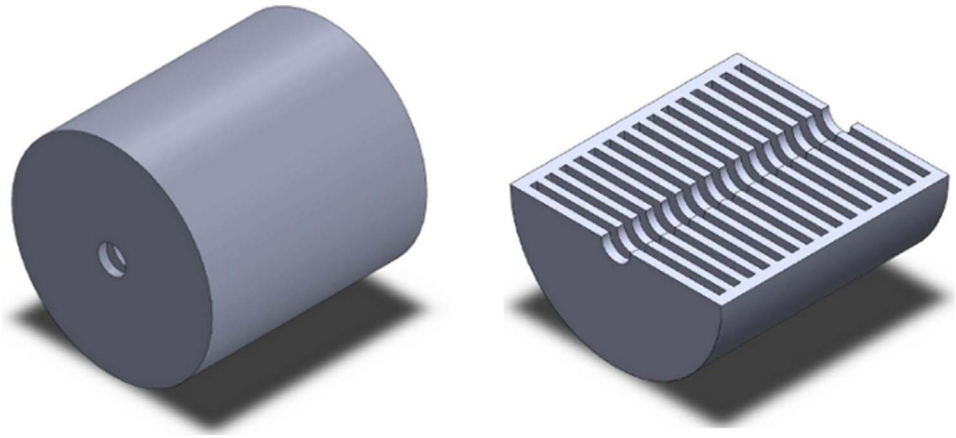

Fig. 2. Prototype sample with proposed microstructure of DE pores: perforated material with multiple 'pancake' cavities. The full sample is shown on the right and its longitudinal cross section is on the left. The parameters of this sample are as follows: the total thickness of the sample is $L = 31$ mm, the external diameter of the cross section of the sample is $d_{samp} = 29$ mm, the main pore diameter is $d_{mp} = 4$ mm, the DE cavity diameter is $d_{de} = 26$ mm, the thickness of the DE cavity is $h_{de} = 1$ mm, the period is $h = 2$ mm, the number of unit cells is $N = 15$.

order to minimize f_{res1}, it is necessary to optimize the effective compressibility C_{de} of the DE pores and to increase the volume ratio V_{de}/V_{mp} of the DE pores and the main pore. As the thermal effects are the key to the performance, it is proposed to take the design of the thermal-exchanger as inspiration. In this design, the DE pores are replaced by very thin lateral cavities ("pancake cavities") and thus a multi-pancake cavity material is designed which is perforated by a main pore (see Fig. 2). Another name could be a "mille-feuille" (a French cake made of alternate thin layers of cream and pastry). The originality of the microstructure design comes from using cavities with very short cavity thickness to diameter section ratio and large heat exchange surfaces.

Although the proposed microstructure for the DE pores is relatively simple, it needs to be controlled and optimized to achieve l good low frequency performance.

2.2. Sample fabrication

The "perforated pancake absorber" can be built using two different fabrication processes: the fabrication by assembly and the one block fabrication (by using a 3D printing technology). For example, this material can be obtained very easily by assembling successively washers and seals with same external diameter and different internal diameters (see Fig. 3). However, to optimize the microstructure, it is recommended to use the one block fabrication process (see Fig. 3). The samples presented in this paper were made by the one block fabrication process.

Two kinds of prototype are presented in this article; both were designed to be tested in the impedance tube. Two different external diameters are proposed; $d_{samp} = 29$ mm and $d_{samp} = 44.4$ mm, corresponding to the two acoustic tubes' cross-section diameters. Both samples have thickness $L = 31$ mm, the same number of periodic cells, the same main pore geometry, the same pancake cavity thickness and the same periodicity. Only the sample diameter and the pancake cavity diameter are modified. Table 1 summarizes the sample parameters.

3. Lumped parameter model with Transfer Matrix formulation

In Ref. [10], the use of the Transfer Matrix Method (TMM) was suggested for modelling the acoustic behavior of air-saturated porous material with periodically distributed dead-end pores. Contrary to the effective fluid approach, TMM is not restricted by the low frequency range. It was also noted in Ref. [5] that the continuous model and the lumped parameter model can be applied to slow sound material. It is proposed here to use the lumped parameter approach with a transfer matrix formulation. The lump element is used here to account for the pancakes cavities located in parallel to the main pore. First, we consider a single cell with thickness h (period) composed of a main pore and a pancake cavity. The common pore, which corresponds to the common volume between the main pore and the pancake cavity, is defined. Thus the single periodic cell is split up in two half main pores (with a thickness $h_{mp}/2$), a common pore and a pancake cavity (with a thickness h_{de}) (see Fig. 4).

The two halves of the main pores are identified as effective fluids with parameters (k_{mp}, Z_{mp}) given by JCA model [1]. It is assumed that Re $(k_{mp}d_{mp}) \ll 1$ so that the wave inside the main pores can be considered plane. The effective fluid parameters of the main pore are given in Table 2. The transfer matrix of a main pore for a thickness $h_{mp}/2$ is given by:

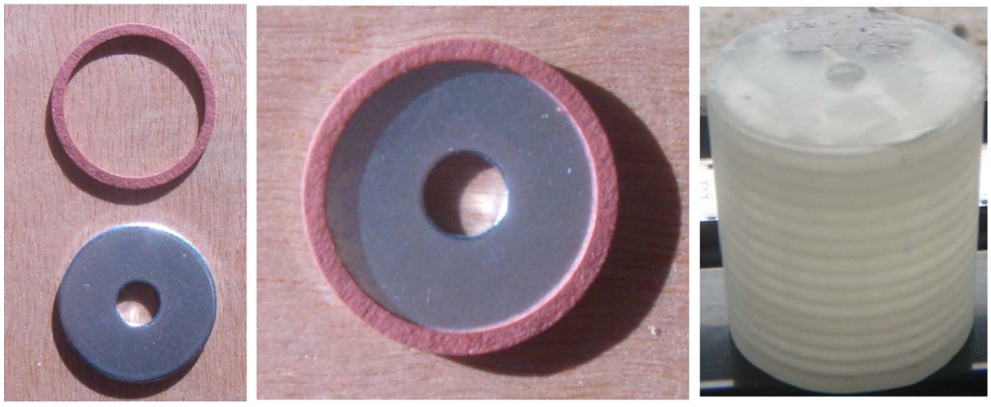

Fig. 3. Example of sample with multiple "pancake" cavities a) and b) "handmade" sample, this sample had been made by assembling washers and seals, c) 3D printing sample (one block fabrication process), this sample has been made using transparent resin (stereo lithography process).

Table 1
Parameters of the multi-pancakes samples.

Samples	Sample diameter d_{samp} (mm)	Main pore diameter d_{mp} (mm)	Pancake cavity diameter d_{de} (mm)	Main pore thickness h_{mp} (mm)	DE pore thickness h_{de} (mm)	Cell number N	Sample thickness L (mm)
Sample A	29	4	26	1	1	15	31
Sample B	44.4	4	40	1	1	15	31

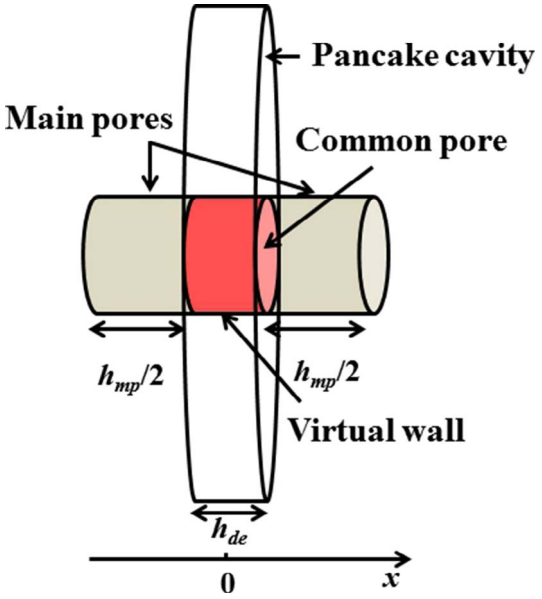

Fig. 4. One single periodic cell composed of two halves of the main pore, a common pore and a "pancake" cavity. The common pore corresponds to the common volume between the main pore and the "pancake" cavity.

$$\mathbf{T}_{mp}^{(h_{mp}/2)} = \begin{pmatrix} \cos(k_{mp}h_{mp}/2) & jZ_{mp}\sin(k_{mp}h_{mp}/2) \\ \frac{j}{Z_{mp}}\sin(k_{mp}h_{mp}/2) & \cos(k_{mp}h_{mp}/2) \end{pmatrix}, \tag{7}$$

time dependence $e^{j\omega t}$ is assumed throughout. The pancake cell is composed by a common pore (identified as a "junction volume" in Ref. [12]) and a truncated pancake cavity (the remainder of the cell), the two elements are separated by a virtual wall (identified as "curtain area" in Ref. [12]). So, the common pore has no lateral rigid wall. In this way, it is proposed to identify the common pore as an element without thermo-viscous losses, thus the transfer matrix of this common element for a thickness $h_{de}/2$ is given by:

$$\mathbf{T}_{com}^{(h_{de}/2)} = \begin{pmatrix} \cos(k_0 h_{de}/2) & jZ_0\sin(k_0 h_{de}/2) \\ \frac{j}{Z_0}\sin(k_0 h_{de}/2) & \cos(k_0 h_{de}/2) \end{pmatrix}, \tag{8}$$

with (k_0, Z_0) are the wavenumber and the characteristic impedance of the air.

Then the pancake cavity is identified as a side branch (same as a DE pore) which is represented by a surface impedance $Z_{S,de}$. It is proposed to use the "pancake" cavity surface impedance expression proposed by Dickey and Selamet [12], valid for circular cross section, to model a Helmholtz resonator (one open-closed cavity) with a small cavity length-to-diameter ratio. Our material is different inasmuch as it is constituted of the series of open-open pancake cavities. In the TMM approach, we propose to use the same expression as in Ref. [12] (adapted with effective parameters) for the surface impedance of a single pancake cavity;

$$Z_{S,de} = jZ_{de}\left\{\frac{H_0^{(1)}(k_{de}r_{mp}) - [H_1^{(1)}(k_{de}r_{de})/H_1^{(2)}(k_{de}r_{de})]H_0^{(2)}(k_{de}r_{mp})}{H_1^{(1)}(k_{de}r_{mp}) - [H_1^{(1)}(k_{de}r_{de})/H_1^{(2)}(k_{de}r_{de})]H_1^{(2)}(k_{de}r_{mp})}\right\}, \tag{9}$$

with $H_i^{(n)}(kr)$ the Hankel function of ith order and of nth kind:

$$H_i^{(1)}(kr) = J_i(kr) + jY_i(kr), H_i^{(2)}(kr) = J_i(kr) - jY_i(kr), \tag{10}$$

with J_i and Y_i are the Bessel functions of first and second kinds and of ith order. The effective parameters (k_{de}, Z_{de}) of air in the pancake cavity are calculated using JCA model. It is assumed here that $h_{de} \ll r_{de} \ll \lambda$, so the expressions for slit geometry are used (Table 2).

At the centre of the common pore ($x = 0$ on Fig. 4), the admittance relation is applied (applying the pressure and volume velocity continuities). The pancake cavity surface impedance $Z_{S,de}$ is applied at the area of the virtual wall separating the common pore and the pancake cavity $A_{de} = 2\pi r_{mp}h_{de}$ (called the "curtain area" in Ref. [12]).

The transfer matrix of the side branch is given by:

$$\mathbf{T}_{de} = \begin{pmatrix} 1 & 0 \\ \frac{1}{Z_{S,de}}\frac{A_{de}}{A_{mp}} & 1 \end{pmatrix}, \tag{11}$$

with $A_{mp} = \pi r_{mp}^2$ the cross-section area of the main pore.

The transfer matrix of the periodic cell with thickness $h = h_{mp} + h_{de}$ is given by:

$$\mathbf{T}_{cell} = \mathbf{T}_{mp}^{(h_{mp}/2)}\mathbf{T}_{com}^{(h_{de}/2)}\mathbf{T}_{de}\mathbf{T}_{com}^{(h_{de}/2)}\mathbf{T}_{mp}^{(h_{mp}/2)}, \tag{12}$$

We consider a sample of material with N periodic cells. The transfer matrix is given by:

$$\mathbf{T}_{samp} = \mathbf{T}_{\phi}\mathbf{T}_{end}(\mathbf{T}_{cell})^N\mathbf{T}_{end}\mathbf{T}_{\phi}^{-1}, \tag{13}$$

with $\mathbf{T}_{end}$ the transfer matrix of the end element which includes the pore end effect, $\mathbf{T}_{\phi}$ is the contraction transfer matrix which are given by:

$$T_{end} = \begin{pmatrix} \cos(k_{mp}h_{end}) & jZ_{mp}\sin(k_{mp}h_{end}) \\ \frac{j}{Z_{mp}}\sin(k_{mp}h_{end}) & \cos(k_{mp}h_{end}) \end{pmatrix}, \tag{14}$$

and

$$\mathbf{T}_{\phi} = \begin{pmatrix} 1 & 0 \\ 0 & MA_{mp}/A_{sample} \end{pmatrix}, \tag{15}$$

where h_{end} is the main pore added length (the end-effect correction is

Table 2
Johnson-Champoux-Allard (JCA) parameters of the main pore and pancake cavity, with η the dynamic viscosity of air.

	Viscous length Λ (μm)	Thermal length Λ' (μm)	Tortuosity α_∞	Static air flow resistivity σ (Pa·s/m^2)	Open porosity ϕ (%)
Main pore (Identified to a circular cross section pore)	r_{mp}	r_{mp}	1	$\frac{8\eta}{r_{mp}^2\phi}$	1
"Pancake" cavity (Identified to a slit)	h_{de}	h_{de}	1	$\frac{12\eta}{h_{de}^2\phi}$	1

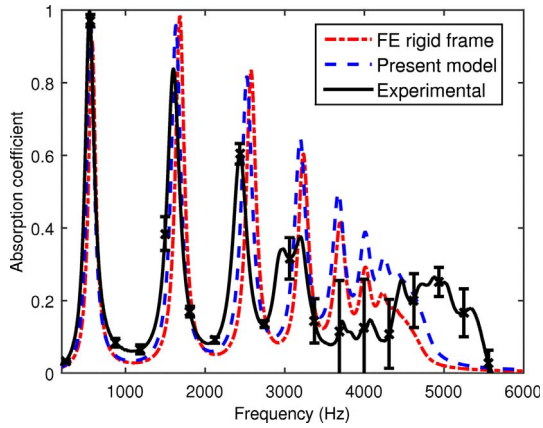

Fig. 5. Normal incidence sound absorption coefficient (sample backed by a rigid wall) of sample *A* (perforated multi-pancake cavity with 29 mm external diameter), the three curves correspond to: results measured in the impedance tube (- - -), results simulated by the transfer matrix approach (-·-·-), results simulated by Finite Element approach (-.-.-) (rigid frame assumption).

given by Eq. 9.18 in Ref. [1]), M is the number of main pores for a sample and A_{sample} is the cross section area of the sample.

The normal incidence sound absorption coefficient of the absorber are then calculated using the elements $t_{samp,ij}$ of matrix (13). The coefficient of the rigidly backed sample (the main pore is in open-closed configuration) is given by:

$$\alpha_N = 1 - \left| \frac{t_{samp,11} - t_{samp,21} Z_0}{t_{samp,11} + t_{samp,21} Z_0} \right|^2 . \tag{16}$$

Remark: note that this material can be also used in transmission configuration (this corresponds to the configuration in which the sample is coupled to two semi-infinite regions, the main pore is in open-open configuration), and in this configuration, the sound transmission loss in normal incidence is directly given by:

$$TL = -20\log_{10} \left| \frac{2}{t_{samp,11} + t_{samp,22} + t_{samp,12}/Z_0 + t_{samp,21} Z_0} \right|, \tag{17}$$

This article concentrate on sound absorption and the transmission configuration will not be presented.

4. Results

4.1. Validation set up

4.1.1. Experimental approach – the impedance tube

The acoustic properties of "perforated pancake absorbers" are measured in two different impedance tubes with diameters d_{tube} = 29 and 44.4 mm. The three-microphone method [16] is used for the tube with d_{tube} = 44.4 mm and the four-microphone method [17,18] is used for the tube with d_{tube} = 29 mm. The frequency ranges were chosen to make sure that only plane waves exist in the tube (between 100 Hz and 6400 Hz for the acoustic tube with the diameter d_{tube} = 29 mm and between 100 Hz and 4200 Hz for the acoustic tube with the diameter d_{tube} = 44.4 mm). The sound pressure excitation is random noise and the set up works in a linear regime. Each sample has been tested twice, interchanging the front and the back surfaces, and several samples have been tested. The results have been averaged over several measurements. Then the results are presented with the mean value $\bar{x}$ and the expanded uncertainty [19] with a coverage factor $h = 1$: $x = \bar{x} \pm h\sigma_x$, with σ_x the standard deviation.

The absorption coefficient results are presented for the configuration in which the sample is backed by a rigid wall.

4.1.2. Numerical approach – the acoustic virtual tube

It is also proposed to compare the semi analytical results of TMM with those obtained numerically (virtual measurements). The virtual measurements are obtained with a three dimensional acoustical FEM simulations using COMSOL Multiphysics software. A three-microphone method [16] is used to get the virtual measurements. In the FEM model, parabolic tetrahedral elements were used to mesh the different acoustic domains of the tube, and convergence of the results was verified in the frequency range of interest (it has been applied a criterions on the element size of at least $d_{el} < \lambda_{min}/15$ where λ_{min} is the minimal wavelength in the material (corresponding to the maximum frequency of the study). The elements of the absorbers were modeled as those filled with effective fluids with complex sound speed ($c_{eff} = \omega/k_{eff}$) and dynamic density ($\rho_{eff} = Z_{ceff}\, k_{eff}/\omega$) given by JCA model as outlined in Table 2. Plane wave in normal incidence is chosen for the acoustic excitation. In this section two numerical models are proposed: a model with rigid frame assumption (the fluid of each element are described by c_{eff} and ρ_{eff}) and a model with elastic frame assumption (considering the vibration of the frame and the fluid-structure interactions). For the model with elastic frame assumption, the fluid elements are described by c_{eff} and ρ_{eff} and the elastic solid elements are described by the Young's modulus E, the Poisson's ratio ν and the density ρ_s of the material.

4.2. Comparison between experimental results and models

4.2.1. Sample A

The measured and simulated normal incidence sound absorption coefficient of the rigidly backed sample *A* (with thickness L = 31 mm, external diameter d_{samp} = 29 mm and pancake cavity diameter d_{de} = 26 mm) are presented in Fig. 5. The first absorption peak is high (close to 100%) and its frequency is around 550 Hz. This frequency is equal to the first resonance frequency of a perforated material without pancake cavities (quarter-wavelength tube resonance) with a thickness $L^* = 4.8\, L$ = 148 mm. Thus, for these samples adding periodic array of pancake cavities allows reduction in thickness by a factor of 4.8. The first resonance of the perforated sample without pancake cavities with same thickness L = 31 mm is $f_{res}* = 2578$ Hz (equivalent as a quarter-wave tube see Section 4.3).

The agreement between the models and the experiments is very good for the first absorption peak (see Table 3 for the values of the frequency and the amplitude of the first and the second sound absorption peaks). For the second and the third absorption peaks, the models predict a slightly smaller frequency shift than observed and overestimate the amplitudes. Above 2500 Hz, both models fail to

Table 3
Mean frequency values and mean amplitudes of the first and the second absorption peaks for samples *A*. The results are given for the experimental approach, the present model and the two FEM models (with rigid frame assumption and with elastic frame assumption).

	Frequency (Hz) 1st peak	Amplitude (%) 1st peak	Frequency (Hz) 2nd peak	Amplitude (%) 2nd peak
Experimental	550	99.7	1603	83.8
Present model	560	97.8	1634	95.8
FEM model (rigid frame)	580	91.9	1680	98.4
FEM model (elastic frame)	580	88.7	1680	98.8

correctly predict the acoustic behavior of the tested sample. The discrepancies are thought to be caused by several effects including the resonance effect due to elasticity of the material and stopband effects occurring in certain frequency bands. The agreement between the present TMM model and the numerical (FE) model is reasonably good in the studied frequency range. However, a noticeable difference is found on the absorption peak frequencies and amplitudes (see Table 3), especially above 3000 Hz. This discrepancy could be explained by the fact that plane wave assumption has been considered in the analytical model.

Moreover due to periodicity of the pore structure, it can be observed that the models predict a stopband above 4700 Hz (the stopband corresponds to absorption coefficient going to zero). On the contrary, the analysis of the measured absorption coefficient shows that there are two stopband effects; one is between 2700 Hz and 4700 Hz and the second is above 4700 Hz. The rigid frame assumption has been considered in the two models (analytical and numerical). To attempt to explain the two observed stop bands on experiments it is proposed here to use a numerical model with elastic frame assumption (COMSOL Multiphysics software with vibro-acoustic option). Mechanical parameters of the Acrylonitrile Butadiene Styrene (ABS); with the density $\rho_s = 1040\,\mathrm{kg/m^3}$, the Young's modulus $E = 2275 \times 10^6\,\mathrm{Pa}$, and the Poisson's ratio $\nu = 0.35$ were used in the model. The comparisons between the experimental results and the two numerical models (with rigid and elastic frame assumptions) are shown in Fig. 6. Accounting for frame elasticity changes the results considerably, leading to appearance of the frequency range (approximately between 3.5 kHz and 4.2 kHz) of low absorption coefficient. It would appear that there would therefore two bandgap effects; the first one corresponding to a vibrational bandgap effect (vibrational resonance of the membrane in periodic array arrangement [20]) and the second one corresponding to an acoustic bandgap effect (acoustic resonance of the pancake cavities in periodic array arrangement). Indeed the first natural frequency of flexural vibrations of a circular ABS plate (similar to the wall between two pancake cavities) is found *in vacuo* condition between 2149 Hz (with "simply supported" boundary conditions) and 4383 Hz (with "clamped" boundary conditions). These natural frequencies are calculated by the approach proposed by Zagrai and Donskoy [22]. The real boundary conditions for the wall of pancake cavities are between "simply supported" and "clamped". Thus the first natural frequency of flexural vibrations is included in the first bandgap frequency bandwidth. Moreover the first acoustic resonance of the pancake cavity is 5239 Hz; this frequency is included in the second bandgap frequency bandwidth. It can be noticed that similar two bandgap effects have been

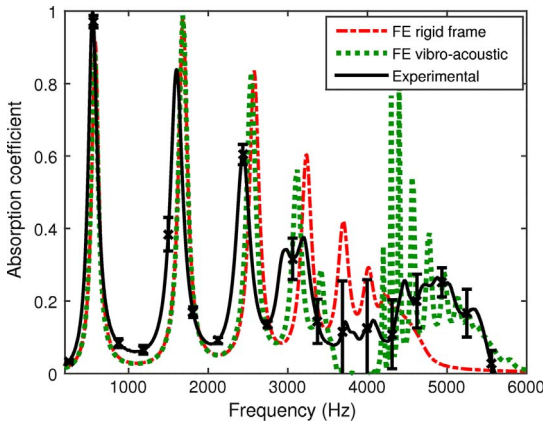

Fig. 6. Normal incidence sound absorption coefficient (sample backed by a rigid wall) of the sample *A* (perforated multi-pancake cavity with 29 mm external diameter). The three curves correspond to: results measured in the impedance tube (- - -), results simulated by Finite Element approach with rigid frame assumption (-.-.-), results simulated by Finite Element vibro-acoustic approach (with elastic frame) (. . .).

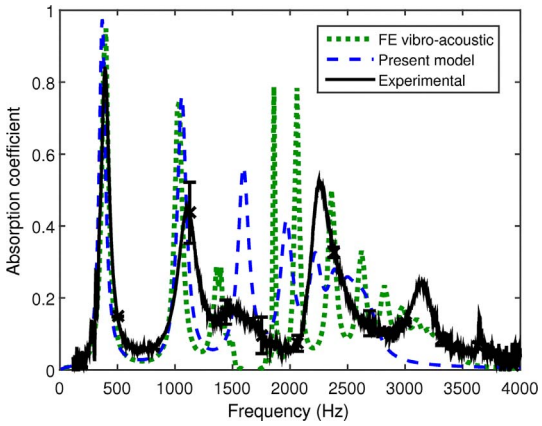

Fig. 7. Normal incidence sound absorption coefficient (sample backed by a rigid wall) of sample *B* (perforated multi-pancake cavity with 44.4 mm external diameter). The three curves correspond to: results measured in the impedance tube (- - -), results obtained using transfer matrix approach (-·-·-), results obtained using Finite Element vibro-acoustic approach (with elastic frame) (. . .).

observed for an acoustic metamaterial composed of a periodically arranged Helmholtz resonators and membranes [23].

4.2.2. Sample B

For sample B, the diameter has been increased in order to increase the pancake cavity volume, increase the effective compressibility (see Eq. (3)) and therefore decrease the first absorption peak (see Eq. (6)). The measured and calculated acoustic properties of sample *B* (with thickness $L = 31$ mm, external diameter $d_{samp} = 44.4$ mm, and pancake cavity diameter $d_{de} = 26$ mm) are presented in Fig. 7. The numerical results are obtained assuming rigid frame and elastic frame. For sample *B,* the pancake cavity diameter is $d_{de} = 40$ mm. The first absorption peak is observed around 392 Hz (see Table 4), which means that adding periodic array of pancake cavities allows reduction in thickness by factor 6.6 compared to simply perforated sample (quarter-wavelength tube), moreover the amplitude of the absorption peak is preserved (see Section 4.3).

Note that when the two bandgap effects occur (for frequencies range between 1500 and 2000 Hz and for frequencies above 2500 Hz), the absorption coefficient decreases significantly, and the sample loses its absorption properties. Thus, the larger the pancake cavity, the lower the band gap frequency is. Indeed, for the larger cavity, the first natural frequency of flexural vibrations of the separating wall is lower and the first acoustic resonance of the "pancake" occurs at lower frequency. For the development of this kind of absorbing material, this point has to be considered in the parameter optimization process.

4.3. Discussion

It can be noticed that for a sample with same parameters as sample *B* but with an external diameter $d_{samp} = 100$ mm and a pancake cavity diameter $d_{de} = 98$ mm, the TMM and FEM models predict the first absorption peak of high amplitude around 184 Hz. Thus, in this case, the periodic array of pancake cavities allows reduction in thickness by factor 14 compared to simply perforated sample.

It is proposed in this part a comparisons between different sound absorbers. A series of comparisons between multi-pancake materials, equivalent Helmholtz Resonator (HR) (with the same thickness and the same cross section area as multi-pancake sample - same overall volume) and a quarter-wavelength tube has been performed. The Helmholtz Resonator study has been done using semi-analytical approaches [3,21]. The equivalent Helmholtz resonator is composed by one main pore h_{mp} and a cylindrical air cavity (with a depth which is given by $L - h_{mp}$, and a section area which is given by: πr_{DE}). Comparisons with

Table 4
Mean frequency values and mean amplitudes of the first and the second sound absorption peaks for sample B. The values are given for the experimental results, the transfer matrix model and the FEM models (with rigid frame assumption and with elastic frame assumption).

	Frequency (Hz) 1st peak	Amplitude (%) 1st peak	Frequency (Hz) 2nd peak	Amplitude (%) 2nd peak
Experimental	368	97.3	1109	45.1
Present model	392	83.8	1060	76.0
FEM model (elastic frame)	400	94.9	1040	74.8

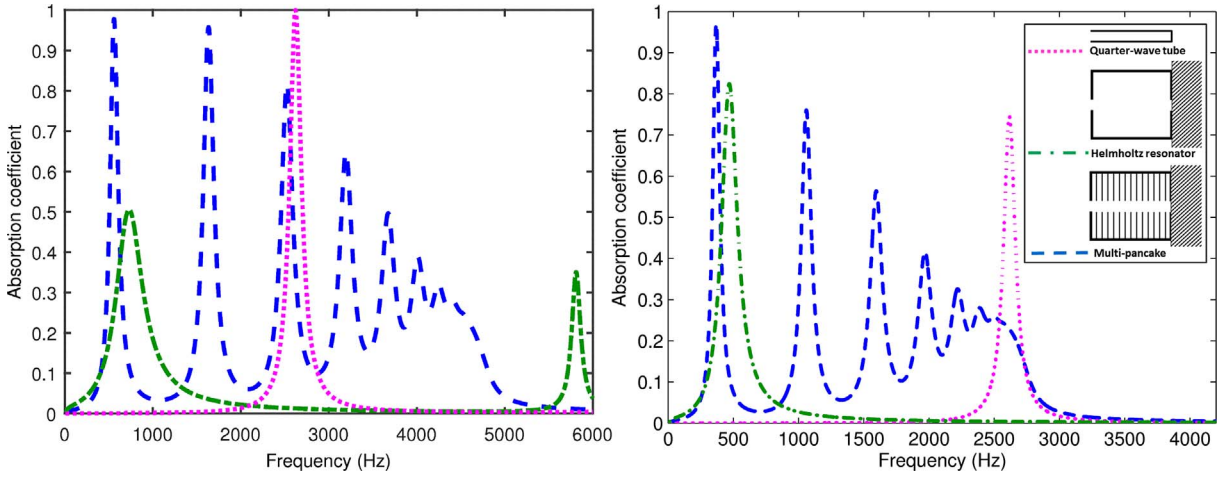

Fig. 8. Comparisons on predicted normal incidence sound absorption coefficient (sample backed by a rigid wall) of (a) multi-pancake sample *A* (with pancake-cavity diameter $d_{de} = 26$ mm) in acoustic tube with 29 mm cross section diameter and (b) multi-pancake sample *B* (with $d_{de} = 40$ mm) in acoustic tube with 44.4 mm cross section diameter (- - -), a Helmholtz resonator (-.-.-) and a quarter-wave tube resonator (. . .).

multi-pancake sample *A* and sample *B* are shown in Fig. 8. In these two cases, a simple Helmholtz resonator (with the equivalent parameters) or a quarter-wavelength tube resonator does not provide an efficient absorption at low or medium frequencies. From the comparisons on samples with same overall volume (that means multi-pancake sample vs HR) it can be noticed the importance and the benefit of the periodic array of DE pores for the low frequency sound absorption (for the frequency and the amplitude of the absorption peaks). As it has been mentioned before the periodic array of pancake cavities allows reduction in thickness by factor 4.8 for sample *A* (with pancake cavity diameter $d_{de} = 26$ mm) and by factor 6.6 for a sample *B* (with $d_{de} = 40$ mm) compared to the wavelength tube resonator. Moreover, contrary to the Helmholtz Resonator and quarter-wavelength tube, the multi-pancake samples allow an array of secondary absorption peak of in mid-frequency range.

However, It can be noticed that the proposed multi-pancake samples are not as effective in mid and high frequencies as classical porous foam (with same thickness) [1]. As it was proposed for sound-absorber composed by porous material with inclusion of Helmholtz Resonator [24], an sound-absorber composed by a multi-pancake sample inserted in a porous media (as melamine foam) could be an efficiently large frequency bandwidth sound absorber.

5. Conclusions

Based on the low frequency approximation of effective parameters of a structured perforated material containing periodically spaced dead-end pores, a microstructure design for low frequency sound absorber materials is proposed in this work. It corresponds to a perforated material with a periodic lattice of internal “pancake” cavities. Sound absorber prototypes have been made and tested in the impedance tube. The periodic lattice of “pancake” cavities allows decreasing significantly the frequencies of the absorption peaks without increasing the thickness of the sample. The amplitude of the absorption peak is preserved. Moreover two stopband effects have been observed for these materials at higher frequencies: the first stopband is due to the acoustic resonance of the periodic pancake cavities and the second to the frame resonance of the sample. Within the stopband frequency ranges, the absorption properties of the absorber decrease in a significant way, so that the stopband effect has to be taken into account in the sound absorber design optimization. To model the acoustic behavior, it is proposed to use a lumped model approach with matrix transfer formulation. The agreement between semi-analytical and numerical approaches and the impedance tube measurements is good for low frequencies. For high frequencies, the vibration of the sample frame has to be taken into account in the models. The next step consists in the optimization of the microstructure to improve the low frequency absorption properties of the proposed sound absorber. Studies are in progress in order to enlarge the absorber frequency bandwidth (especially at mid and high frequencies) and to optimize the frequency value of the first absorption peak (lower as possible).

References

[1] Allard JF, Atalla N. Propagation of sound in porous media: modelling sound absorbing materials. 2nd ed. New York: John Wiley and Sons; 2009.
[2] Ingard U. On the theory and design of acoustic resonators. J Acoust Soc Am 1953;25(6):1037–106.
[3] Maa DY. Microperforated-panel wideband absorbers. Noise Control Eng J 1987;29(3):77–84.
[4] Ruiz H, Cobo P, Dupont T, Martin B, Leclaire P. Acoustic properties of plates with unevenly distributed macro perforations backed by woven meshes. J Acoust Soc Am 2012;132:3138–47.
[5] Aurégan Y, Farooqui M, Groby JP. Low frequency sound attenuation in a flow duct using a thin slow sound material. J Acoust Soc Am 2016;139:EL149.
[6] Li D, Chang D, Liu B. Enhancing the low frequency sound absorption of a perforated panel by parallel-arranged extended tubes. Appl Acoust 2016;102:126–32.
[7] Lagarrigue C, Groby J-P, Tournat V, Umnova O. Absorption of sound by porous layers with embedded periodic array of resonant inclusions. J Acoust Soc Am 2013;134:4670–80.
[8] Boutin C. Acoustics of porous media with inner resonators. J Acoust Soc Am 2013;134:4717.
[9] Bradley CE. Time harmonic Bloch wave propagation in periodic waveguides. Part I.

Theory. J Acoust Soc Am 1994;96:1844–53.
[10] Leclaire P, Umnova O, Dupont T, Panneton R. Acoustical properties of air-saturated porous material with periodically distributed dead-end pores. J Acoust Soc Am 2015;137(4):1772–82.
[11] Groby J-P, Huang W, Lardeau A, Aurégan Y. The use of slow waves to design simple sound absorbing materials. J Appl Phys 2015;117:124903.
[12] Dickey NS, Selamet A. Helmholtz resonators: one-dimensional limit for small cavity length-to-diameter ratios. J Sound Vib 1996;195(3):512–7.
[13] Leclaire P, Dupont T, Aivazzadeh S, inventors, Universite de Bourgogne, assignee. Resonateur acoustique de faible epaisseur de type mille-feuille perfore pour l'absorption ou le rayonnement acoustique tres basses frequences (Low thickness perforated mille-feuille acoustic resonator for absorbing or radiating very low acoustic frequencies). International patent WO 2017134125 A1; 2017 Aug 10.
[14] Sheng P. Introduction to wave scattering, localization and mesoscopic phenomena. Berlin: Springer; 2006. p. 61.
[15] Champoux Y, Allard JF. Dynamic tortuosity and bulk modulus in air-saturated porous media. J Appl Phys 1991;70:1975–9.
[16] Salissou Y, Doutres O, Panneton R. Complement to standard method for measuring normal incidence with three microphones. J Acoust Soc Am 2012;131:EL216.
[17] ASTM E 2611-09. Standard test method for measurement of normal incidence sound transmission of acoustical materials based on the transfer matrix method.
[18] ISO 10534-2. Acoustics—determination of sound absorption coefficient and impedance in impedance tubes. Part 2: transfer-function method. Geneva (Switzerland): International Organization for Standardization; 1998.
[19] Joint Committee for Guides in Metrology. Evaluation of measurement data-guide to the expression of uncertainty in measurement (JCGM 100:2008, Bur. Intl. Poids et Mesures, Sèvres, 2008).
[20] Lee SH, Park CM, Seo YM, Wang ZG, Kim CK. Acoustic metamaterial with negative density. Phys Lett A 2009;373:4464.
[21] Atalla N, Sgard F. Modeling of perforated plates and screens using rigid frame porous models. J Sound Vib 2007;303:195–208.
[22] Zagrai A, Donskoy D. A soft table for the natural frequencies and modal parameters of uniform circular plates with elastic edge support. J Sound Vib 2005;287:343–51.
[23] Seo YM, Park JJ, Lee SH, Park CM, Kim CK. Acoustic metamaterial exhibiting four different sign combinations of density and modulus. J Appl Phys 2012;111:023504.
[24] Doutres O, Atalla A, Osman H. Transfer matrix modeling and experimental validation of cellular porous material with resonant inclusions. J Acoust Soc Am 2015;137(6):3502–13.